ACS Catalysis

Research Article

pubs.acs.org/acscatalysis

Active Site Considerations on the Photocatalytic H_2 Evolution Performance of Cu-Doped TiO_2 Obtained by Different Doping Methods

Juan M. Valero, Sergio Obregón, and Gerardo Colón*

Instituto de Ciencia de Materiales de Sevilla, Centro Mixto Universidad de Sevilla-CSIC, Américo Vespucio s/n, 41092 Sevilla, Spain

Supporting Information

ABSTRACT: A photocatalytic H_2 evolution reaction was performed over copper doped TiO_2. The influence of sulfate pretreatment over fresh TiO_2 support and the Cu doping method has been evaluated. Wide structural and surface characterization of catalysts was carried out in order to establish a correlation between the effect of sulfuric acid treatment and the further Cu-TiO_2 photocatalytic properties. Notably a different copper dispersion and oxidation state is obtained by different metal decoration methods. From the structural and surface analysis of the catalysts we have stated that the occurrence of highly disperse and reducible Cu^{2+} species is directly related to the photocatalytic activity for the H_2 production reaction. Highly active materials have been obtained from a chemical reduction method leading to 18 $mmol \cdot h^{-1} \cdot g^{-1}$ for 3 mol % copper loading.

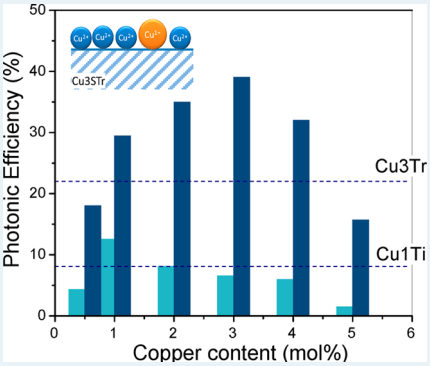

KEYWORDS: *Cu-TiO_2, photocatalysis, active site, sulfation, H_2 evolution*

INTRODUCTION

It has been widely stated that the improvement and optimization of TiO_2 as a photocatalyst is an important task in order to achieve a real application of heterogeneous photocatalysis in the near future.[1] Within this context, the interest in energy related applications of photocatalysis is currently growing.[2] Thus, H_2 production by photoreforming or the synthesis of valuable fuels from CO_2 photoreduction reactions appear as the new challenged topics in this field.[3−5] Taking into consideration the current socioeconomical and environmental situation, it is widely believed that hydrogen will play an important role since it is considered the ultimate clean energy carrier. However, when TiO_2 is exploited in hydrogen production using a photoreforming reaction, some important factors make in principle its application far from a practical situation.[1] In this sense, a rapid recombination process of the photogenerated charge pairs and the occurrence of the eventually backward reactions are considered critical points that might be overcome. Thus, the incorporation of metal ions has been traditionally used as charge trapping sites and avoids the electron−hole recombination processes.[6,7] Among the potential options, noble metals (Pt, Au, Pd) have been widely considered.[8−10] Alternatively, transition metal doping with Cu, Fe, Co, or Ni has recently turned as a promising cheaper option.[11−15] Although the rates obtained are still far from those obtained for noble metals, copper based catalysts appear as a promising candidate. In spite of this, the nature of the active copper species (Cu_2O or CuO) and other external factors governing its photoactivity is less understood.[15] Thus, some authors claimed that Cu_2O species are responsible for the photoactivity for H_2 generation from water reduction.[16,17] Thus, Xi et al. correlated the presence of easily reducible Cu_2O species toward metallic Cu during the H_2 production reaction with the improved photocatalytic activity.[17] On the other hand, other authors argued that the presence of CuO would be responsible for the enhanced separation of photoinduced electrons and holes.[18] Moreover, Ampelli et al. reported the improving effect of Cu^{2+} incorporation into the TiO_2 structure which leads to the creation of oxygen vacancies.[13] Indeed, these authors concluded that embedded CuOx@TiO_2 systems showed higher photocatalytic performances with respect to impregnated samples.[19] Within this context, Korzhak et al. investigated the relationships between the quantum efficiencies of the photocatalytic hydrogen production and the textural characteristics of a Cu-doped TiO_2 system.[20] These authors correlated the photoactivity with the Cu nanostructure obtained specially with deterioration of the electronic interactions between the components of metal−semiconductor composites with growth of the metal nanoparticles size. On this basis, the interaction with TiO_2 is expected to stabilize the copper oxides against photocorrosion and could enhance the activity by a most efficient process. Thus, well dispersed CuOx nanoparticles would be easily reduced during the reaction forming well dispersed copper metal particles which would favor electron trapping.[19]

Received: June 20, 2014
Revised: July 18, 2014
Published: August 15, 2014

   dx.doi.org/10.1021/cs500865y | *ACS Catal.* 2014, 4, 3320−3329

From these considerations, it is assumed that the complex structural, morphological, and chemical features of copper species would strongly affect the final photocatalytic performance for the H_2 production reaction.

In the present paper we try to present an exhaustive structural and surface characterization of different Cu-doped TiO_2 obtained from different doping methods. From the comparison of the chemical features of Cu species we propose a tentative correlation with the final photocatalytic performance for the H_2 production reaction.

EXPERIMENTAL SECTION

Catalysts Preparation and Characterization. The TiO_2 system was prepared by a sol–gel method using titanium tetraisopropoxide (TTIP) as a precursor (10 mL TTIP) in a water/isopropyl alcohol solution (200 mL of iPrOH and 2 mL of H_2O). Forced hydrolysis of the TTIP solution was achieved by adding a certain volume of bidistilled water (8.4 mL). Finally the pH was adjusted to 9 by adding NH_4OH. Copper doping has been performed by means of two different methods: impregnation and chemical reduction.

Impregnated copper doped systems were obtaining by incipient wetness impregnation using $Cu(NO_3)_2$ as a copper precursor dispersed in 1 M H_2SO_4 by means of 2 mL dispersion per gram of fresh TiO_2 (These samples were named as CuXSTi where X is the Cu mol %.). Thus, obtained precursors were then dried at 120 °C overnight. Doped TiO_2 systems were calcined in air at 650 °C for 2 h. In order to discuss the effect of H_2SO_4 impregnation we have also prepared a reference CuXTi catalyst by using water instead of H_2SO_4 in the impregnation step. This reference CuXTi series has been calcined at 400 °C for 2 h. Without sulfate pretreatment, the TiO_2 precursor suffers a rutilization process from the first stage of calcination. For this reason a nonsulfated reference material was submitted to calcination at 400 °C vs 650 °C of a sulfated one. These temperatures correspond to the optimum calcination temperature for nonsulfated and sulfated series (result not shown).[21]

On the other hand, the reduced series has been obtained by chemical reduction of a copper precursor by means of $NaBH_4$. Thus, 1 g of $STiO_2$ or TiO_2 (calcined at 650 and 400 °C, respectively) was dispersed in 100 mL of water solution containing the corresponding stoichiometric amount of copper precursor. Then an excess of $NaBH_4$ was added, and the dispersion was thoroughly stirred for 1 h at room temperature. Finally this solution was filtered and washed with distilled water, and the obtained powder dried at 110 °C overnight.

BET surface area measurements were carried out by N_2 adsorption at 77 K using a Micromeritics 2000 instrument.

X-ray diffraction (XRD) patterns were obtained using a Siemens D-501 diffractometer with Ni filter and graphite monochromator. The X-ray source was Cu Kα radiation. Anatase–rutile fractions were calculated by taking into account the relative diffraction peak intensities. From the line broadening of corresponding X-ray diffraction peaks, we have calculated the mean crystallite size according to the Scherrer equation.

Diffuse reflectance spectra were obtained on a UV–vis scanning spectrophotometer Shimadzu AV2101, equipped with an integrating sphere, using $BaSO_4$ as reference. UV–vis spectra were performed in the diffuse reflectance mode (R) and transformed to a magnitude proportional to the extinction coefficient (K) through the Kubelka–Munk function, $F(R_\infty)$. For the sake of comparison, all spectra were arbitrarily normalized in intensity to 1. Band gap values were obtained from the plot of the modified Kubelka–Munk function $(F(R_\infty)E)^{1/2}$ versus the energy of the absorbed light E.

XPS data were recorded on 4·4 mm^2 pellets, 0.5 mm thick, prepared by slightly pressing the powdered materials which were outgassed in the prechamber of the instrument at 105 °C up to a pressure $<2 \times 10^{-8}$ Torr to remove chemisorbed water from their surfaces. Spectra were recorded using a Leybold-Heraeus LHS-10 spectrometer, working with constant pass energy of 50 eV. The spectrometer main chamber, working at a pressure $<2 \times 10^{-9}$ Torr, is equipped with an EA-200 MCD hemispherical electron analyzer with a dual X-ray source working with Al Kα ($h\nu$ = 1486.6 eV) at 120 W and 30 mA. The C 1s signal (284.6 eV) was used as an internal energy reference in all the experiments.

Transmission electron microscopy (TEM) and scanning electron microscopy (FE-SEM) were performed with Philips CM200 and Hitachi S4800 microscopes, respectively. The samples were dispersed in ethanol using an ultrasonicator and dropped on a carbon grid.

Temperature-programmed reduction (H_2-TPR) experiments were performed using a chemisorption analyzer (Autochem II 2920) and according to the following experimental conditions. A 5% H_2/Ar (20 mL/min) flow was used as the reducing atmosphere from room temperature up to 700 °C, with a heating rate of 10 °C/min and using 300 mg of sample. The H_2 consumption was monitored with a TCD detector, using a CuO reference sample for quantification. In order to avoid high distortions in the TPR profiles, the amount of sample used in each experiment has been calculated by considering the characteristic number K proposed by Monti and Baiker[22]

$$K = \frac{S_0}{F \cdot C_0}$$

where S_0 is the amount of reducible species, and $F \cdot C_0$ is the hydrogen feed to the reactor. These authors proposed that K should be kept between 55 and 140 s for heating rates between 6 and 18 °C/min. In our case, the amount of sample used has been maintained as low as possible, within the limits of experimental sensitivity, and in any case lower than 20K.[23]

Photocatalytic Runs. Photocatalytic H_2 production tests were performed in a flow-reactor system (Figure 1). The

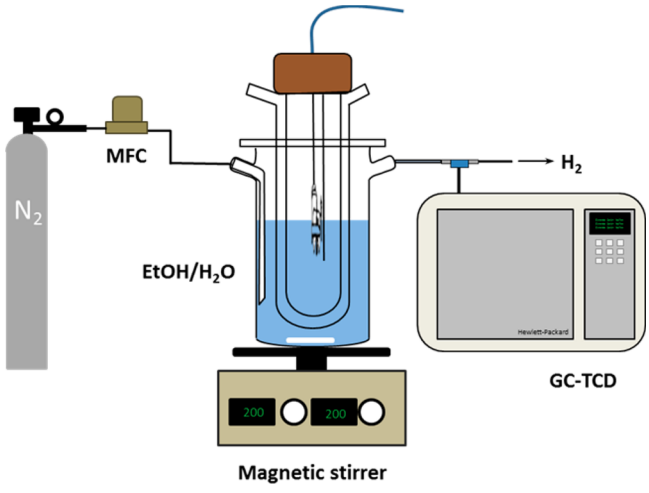

Figure 1. Photocatalytic flow-reactor used for hydrogen production reaction.

dx.doi.org/10.1021/cs500865y | ACS Catal. 2014, 4, 3320–3329

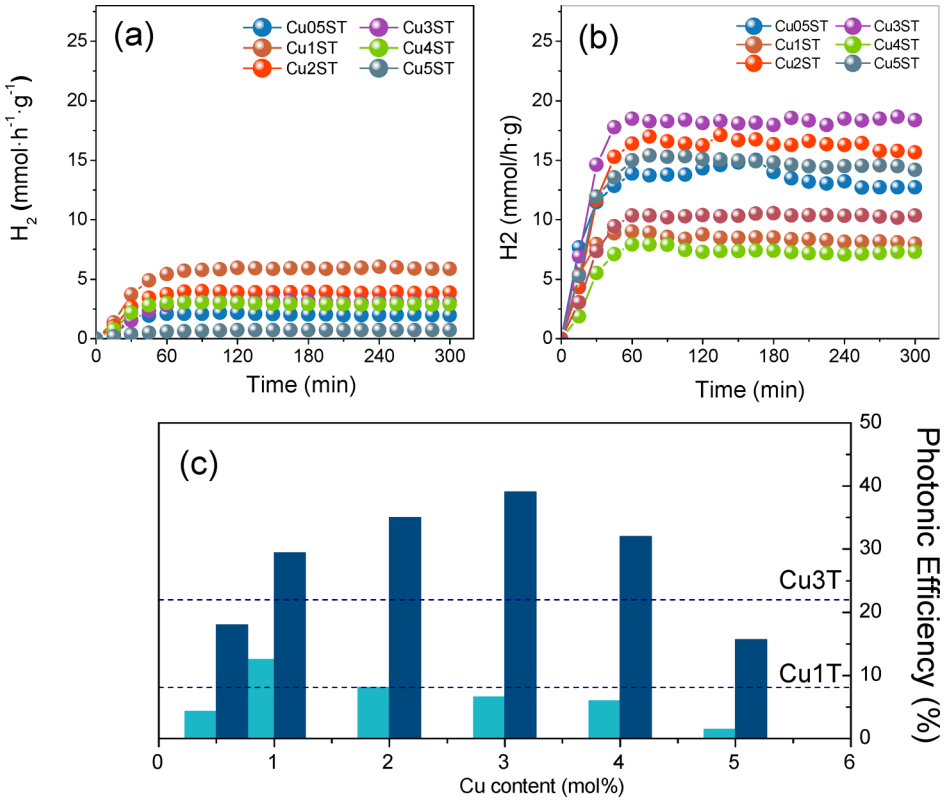

Figure 2. H_2 production for a) CuSTi and b) CuSTr series. c) Calculated photonic efficiencies for Cu-doped TiO_2.

powder photocatalysts were suspended in a methanol−water solution (300 mL, MeOH 10% v/v in water). The reaction media was continuously thermostated at 23 °C ± 2 °C to prevent any significant evaporation of the sacrificial agent. The catalyst suspension (0.5 g/L) was first degassed with an N_2 stream (150 mL/min) for 30 min. After that the N_2 flow was settled at 15 mL/min and stabilized for 15 min. This nitrogen flow was used to displace the hydrogen produced from the photoreactor headspace toward the GC measuring system. Then, the lamp (125 W medium pressure Hg lamp) was switched on, and the effluent gases were analyzed to quantify H_2 production by gas chromatography (Agilent 490 micro GC) using a thermal conductivity detector.

The photonic efficiency for the H_2 evolution reaction has been determined from the reaction rate and the flux of incoming photons (calculated for the irradiation wavelengths of 365 nm) accordingly

$$\zeta(\%) = \frac{rate}{J \cdot A} \cdot 100$$

where the *rate* is the H_2 production rate (mol/s); J = flux of photons (mol/s·m^2); and A = illuminated area (m^2).

The flux of photons was calculated by means of the following equation

$$J = \frac{I \cdot \lambda}{N_A \cdot h \cdot c}$$

where I = light intensity (W/m^2); λ = 365 nm; N_A = Avogadro constant; h = Planck's constant; and c = speed of light (m^2/s).

RESULTS AND DISCUSSION

In Figure 1 we show the H_2 evolution from a methanol/water mixture in the presence of the different CuOx−TiO_2 nanocomposites obtained from different doping methods. As it can be noted the optimum H_2 production rates obtained for impregnated and chemically reduced series are plainly different. Thus, for the impregnated series the optimum Cu doping is 1 mol % for which the H_2 production rate is 6 mmol·h^{-1}·g^{-1} (Figure 2a). On the other side, for the chemically reduced series, the optimum value is attained for 3 mol % of copper (Figure 2b). It is clear that different doping methods strongly affect the reactivity of the systems and lead to a notably different optimum copper loading for this reaction. Moreover, for the CuSTr series, the H_2 production rate is significantly higher than for the impregnated series (18 mmol·h·g^{-1}). It is worthy to note that this H_2 production rate is notably high if compared to those reported in the literature for non-noble metal-based photocatalysts.[11,24−26] By comparing these results of optimum catalysts with the corresponding ones obtained with unsulfated TiO_2 (Cu1Ti and Cu3Tr) it can be evidenced that sulfate pretreatment strongly influences the final photocatalytic performance in both cases. As already stated in previous papers presulfation treatment induces important structural and morphological modifications on TiO_2 which renders improved photocatalytic performances.[27−29] Thus, for the sample obtained by a simple impregnation method (Cu1T) a notably lower photoactivity value is obtained (3.8 mmol·h^{-1}·g^{-1}); similarly a chemically reduced sample using bare TiO_2 leads to lower photoactivity (8.1 mmol·h·g^{-1}) with respect to the optimum value of its series. This fact clearly denotes the crucial role of sulfation in the final performance of the catalysts in both series.

dx.doi.org/10.1021/cs500865y | ACS Catal. 2014, 4, 3320−3329

From reactions rates we have calculated photonic efficiencies for the studied systems (Figure 2c). The obtained values are plainly superior to the actually reported ones (typically below 35%) and would evidence the effect of TiO_2 support as well as the particular characteristic of copper species present.[30,31]

In order to understand the differences in the photocatalytic activity observed we have performed a wide structural and surface characterization of the sulfated series. As it has been previously reported, the sulfation pretreatment over amorphous TiO_2 precursor induces important structural and surface stabilization of anatase upon further calcination.[27] Although a large number of papers reported the use of sulfur as TiO_2 dopant, in our case the structural and surface effect on TiO_2 during calcination is crucial. As already reported by us, the presence of surface sulfur as dopant appears to be detrimental for the photocatalytic activity.[32] Indeed, the best photoactivity is achieved when sulfur residue appears negligible.

Thus, anatase structure remains as the main crystalline phase up to temperatures close to 700 °C. Within the present simultaneous impregnation-sulfation method, the stabilization of anatase structure appears harmed by the presence of copper (Figure 3a). As copper content increases the rutile fraction

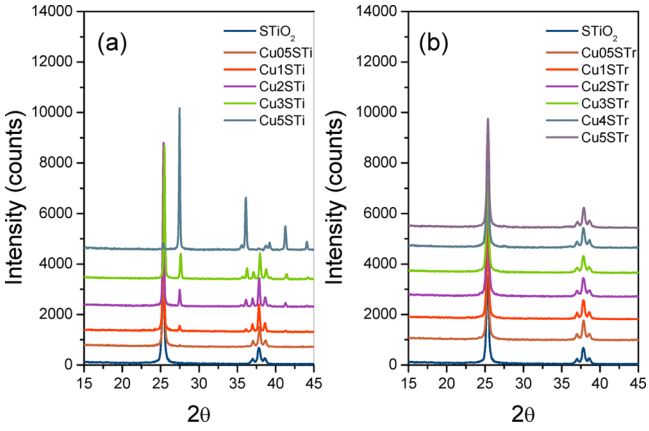

Figure 3. X-ray diffraction patterns for a) CuSTi and b) CuSTr series.

progressively increases reaching for 5 mol % content to the practical rutilization of the system. The rutilization effect of copper appears more evident for the Cu1T sample for which the stabilizing role of surface sulfates is not present (Table 1). For this later sample with only 1 mol % of Cu the rutile fraction rises to 20% vs 4% of rutile calculated for Cu1ST. On the other side, and as expected, the incorporation of copper over calcined $STiO_2$ by chemical reduction does not produce any significant modification of the structural features of TiO_2 (Figure 3b).

By observing the anatase and rutile cell volumes calculated from Rietveld refinement it is clear that while anatase does not change, the rutile cell seems to suffer a slight expansion as Cu loading increases (Table 2). Therefore, as copper content is increased, it can be stated a certain incorporation of the doping ion into the TiO_2 structure. Moreover, this incorporation is taking place preferentially into the rutile crystalline phase, which shows a progressive cell expansion. Once surface sulfates are evolved upon calcination at high temperatures, the rutile crystalline structure drastically rises up. In this case the presence of surface copper hinders the anatase stabilization by sulfates, inducing the progressive rutile appearance. At the same time, from Rietveld refinement it might be assumed that Cu^{2+} insertion is taking place by substitutional doping on the

Table 1. Surface and Structural Properties for Cu-Doped TiO_2 Systems

sample	S_{BET} (m^2/g)	anatase molar fraction	band-gap (eV)	crystallite size (nm)[a]
TiO_2 400 °C	50	100	3.10	21
$STiO_2$ 650 °C	31	100	3.10	26
Cu05STi	14	100	3.07	34
Cu1STi	10	96	3.00	51
Cu2STi	6	90	2.95	53
Cu3STi	5	82	2.91	51
Cu5STi	6	5	2.92	65
Cu05STr	29	100	3.10	29
Cu1STr	28	100	3.10	30
Cu2Tr	31	100	3.00	26
Cu3STr	32	100	3.00	27
Cu5STr	30	100	3.10	26
Cu1Ti	12	80	2.90	21
Cu3Tr	46	100	3.00	19

[a]Anatase crystallite size measured from XRD peak broadening for (101) reflection.

rutile structure. This effect is more pronounced for Cu1T samples, for which the stabilizing effect of surface sulfates is not present. Thus, the rutilization effect is notable with respect to the similar Cu1ST sample. Moreover, by observing the rutile cell parameters it is worthy to note a significant growth in the cell volume (62.51 vs 62.48 for Cu1T and Cu1ST, respectively). This result would point out that the substitutional incorporation of copper into TiO_2 is avoided by surface sulfates which would stabilize the anatase structure as well as copper species at the surface. Thus, the incorporation of copper into the TiO_2 structure leads to a drastic rutilization of TiO_2, being more noticeable in a simply impregnated sample.

Raman spectroscopy is often used for the structural characterization of materials. In particular, this technique is very useful in the case of TiO_2 systems. In our case only Raman peaks corresponding to TiO_2 can be detected (Figure 4). Thus, as copper doping concentration increases it is possible to envisage the appearance of a new set of peaks corresponding to the rutile phase. It has been extensively reported that the anatase Eg peak located at ca. 150 cm^{-1}, associated with O−Ti−O symmetric stretching vibration, is very sensitive to the structural defects present.[33] In this sense, the obtained Raman spectra for the impregnated series denote no shift or broadening in the anatase Eg peak at around 150 cm^{-1} (Figure 4a). It has been stated for Cu-doped TiO_2 systems a clear shift toward a higher Raman shift and a progressive broadening as copper doping increases.[34,35] If doping occurs on substitutional positions of the Ti^{4+} site, the Ti−O−Ti bond will be disturbed by the new Ti−O−Cu or Cu−O−Cu bonds formed. This will affect the peak profile and will be indicative of the presence of a certain structural deformation.[36] In the present case, no significant shift is observed for the CuSTi series. However, for the Cu1T sample it is possible to notice a notable shift with respect to the Cu1STi sample (Figure 4b). Such distortion of the Raman Eg peak for anatase could be directly related to the existence of oxygen vacancies generated in order to conserve the local charge neutrality within the anatase lattice upon Cu^{2+} substitution on Ti^{4+} sites. This would imply that the Cu1T sample would exhibit a more distorted structure caused by Cu doping. Regarding the chemically reduced series, since the

dx.doi.org/10.1021/cs500865y | ACS Catal. 2014, 4, 3320−3329

Table 2. Structural Features from Rietveld Analysis for Cu-Doped TiO_2 Series from a Simultaneous Impregnation-Sulfation Method

	anatase			rutile			
sample	a=b	c	volume	a=b	c	volume	% rutile
TiO_2	3.7865	9.5114	136.37				
$STiO_2$	3.7864	9.5125	136.38				
Cu1STi	3.7854	9.5175	136.38	4.5946	2,9586	62.46	3
Cu2STi	3.7854	9.5174	136.38	4.5949	2,9592	62.48	10
Cu3STi	3.7855	9.5175	136.39	4.5950	2.9595	62.49	20
Cu4STi	3.7859	9.5150	136.38	4.5950	2.9592	62.48	30
Cu5STi				4.5949	2.9592	62.48	95
Cu1Ti	3.7859	9.5142	136.37	4.5951	2.9604	62.51	20

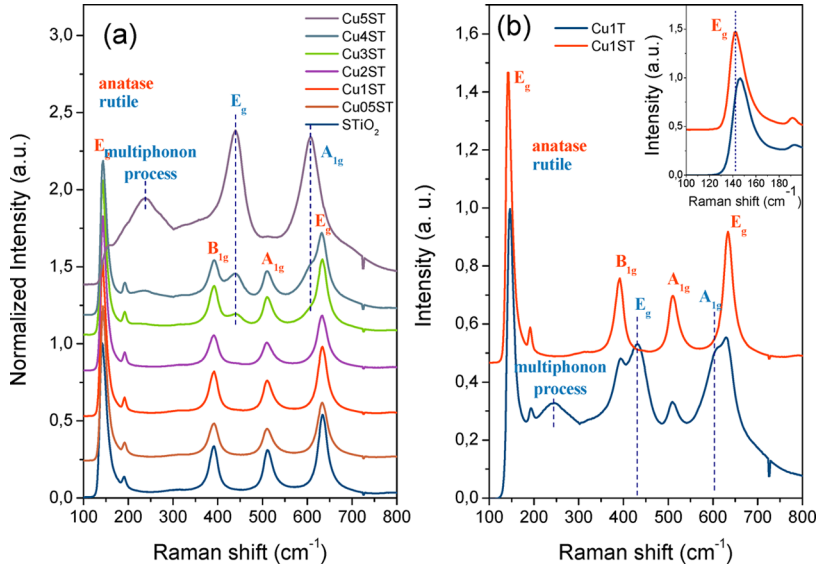

Figure 4. a) Raman spectra for the CuSTi series and b) comparison of Raman spectra for Cu1STi and Cu1Ti samples.

incorporation of copper is only at the surface, no effect on the structure is observed (not shown).

In Table 1 the surface and structural properties of different Cu-TiO_2 systems are summarized. BET surface areas for impregnated series progressively decrease as doping increases. This trend can be correlated with the progressive rutile appearance previously observed for this series. Moreover, a simply impregnated sample shows a drastic BET surface area diminution with respect to an undoped TiO_2 sample. So, it is clear that the copper doping induces a drastic influence in both structure and surface area. Besides, in spite of its lower calcination temperature with respect sulfated series, the Cu1T sample shows a similar BET surface area as the corresponding sample obtained by a simultaneous impregnation-sulfation method, Cu1ST. The chemically reduced series shows in all cases similar surface areas values to the $STiO_2$ reference sample. So, the incorporation of copper does not affect the surface feature in the whole series.

Thus, the two doping methods lead to evident different structural and surface situations. Impregnation previous to calcination induces the progressive rutile appearance and the subsequent loss of surface area. This anatase destabilization is more pronounced when sulfates are not present. On the other side, chemical reduction over just calcined samples does not affect the structural or surface features of the TiO_2 support.

As a consequence, it is expected that the morphology of the studied systems were also influenced by the different impregnation methods. Thus, simultaneous sulfation produces a stabilization of the particle size upon calcination. Cu1ST shows particle aggregates formed by small roundish particles of around 60−80 nm (Figure 5). These aggregates appear to be larger than the reference $STiO_2$. As expected, the Cu3STr sample shows a great similarity in morphology to the parent $STiO_2$ reference. Moreover, the distribution of copper on the particles is highly homogeneous indicating that both impregnation methods lead to a good distribution of dopant on the TiO_2 surface (Figures 6 and S1 in the Supporting Information).

From diffuse reflectance spectroscopy it is possible to envisage the Cu species present (Figure 7). Besides the TiO_2 absorption band it is possible to observe additional absorption contributions associated with CuOx species located in the visible range (400−800 nm).[34,37] It has been described that the band located at 210−270 nm is indicative of the $O^{2-}(2p) \rightarrow Cu^{2+}(3d)$ ligand-to-metal charge-transfer transition, where the Cu ions occupy isolated sites over the support. This band will appear overlapped by the TiO_2 absorption band. Additionally, a band at 350 nm would indicate the formation of Cu^{1+} clusters $(Cu-O-Cu)^{2+}$ in a highly dispersed state.[38] A further band located at 400−500 nm might be assigned to the three-dimensional Cu^{1+} clusters in the CuO matrix due to a partial reduction of Cu^{2+}.[39] The d-d transition of the Cu^{2+} ion in the presence of the ligand (or crystal) field generated by ligand or oxygen ions has been reported to appear in the visible or near-infrared range. Finally, the absorption bands at 600−800 nm

dx.doi.org/10.1021/cs500865y | ACS Catal. 2014, 4, 3320−3329

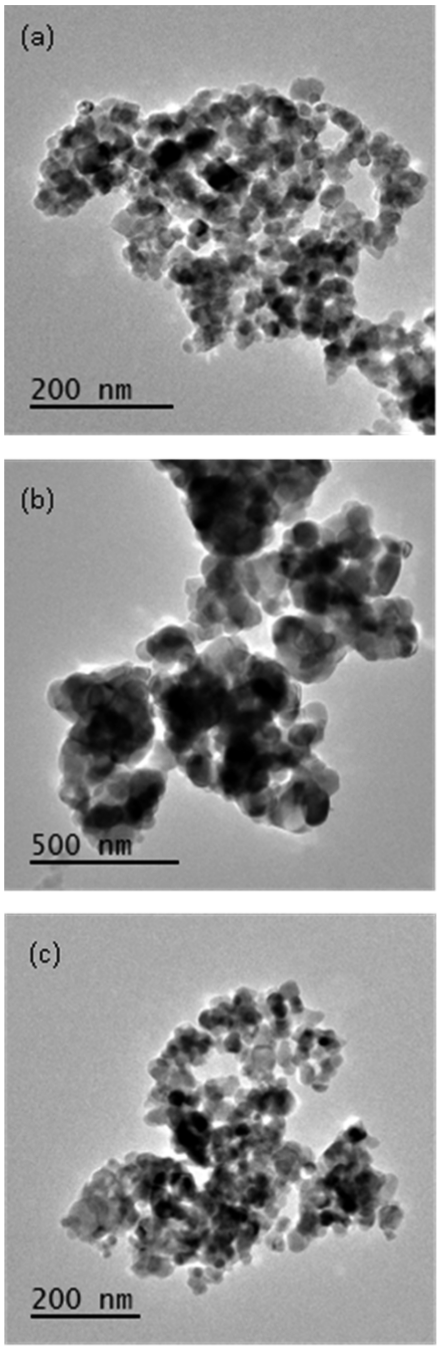

Figure 5. TEM image of a) $STiO_2$, b) Cu1STi, and c) Cu3STr samples.

and 740−800 nm are assigned to $2E_g \rightarrow 2T_{2g}$ transitions of Cu^{2+} located in the distorted or perfect octahedral symmetry (Jahn−Teller effect), respectively.[40]

The evolution of the difference spectra with respect to the reference TiO_2 evidences the different Cu species present in each series (Figure 7). Regarding the impregnated-sulfated series, it can be observed that as copper content increases an emerging peak at ca. 400 nm is formed (Figure 7a). This would indicate the shift in the absorption edge due to the appearance of the rutile phase already mentioned (see band gap values in Table 1).[27] As described in the literature, this band could be also associated with the existence of Cu^{1+} species. Indeed both facts are correlated. Additional small contributions at 420 and ca. 780 nm can be noted. From these bands it can be stated that the CuSTi series exhibits different copper species related to Cu oxidation states in different structural situations. By observing the evolution of the chemically reduced series (Figure 7b) it is worthy to note that the emerging band at around 400 nm associated with the rutile appearance is not present. Moreover new contributions at 440, 500, and 760 nm denote the presence of Cu^{1+} as well as to Cu^{2+}. If we compare the difference spectra for Cu1STr, Cu1STi, and Cu1Ti (Figure 7c), it is worthy to note that for the simply impregnated sample (Cu1Ti) the band at ca. 780 nm is not present, denoting the absence of the dimensionally restricted CuOx clusters. Moreover, it can be observed that bands at 440 and 500 nm are exalted in Cu1T with respect to Cu1STr or Cu1STi. As mentioned, this band can be associated with the presence of Cu^{1+} species.[41] Therefore, it can be assumed that a higher degree of Cu^{1+} is present in Cu1Ti with respect to Cu1STi.

It appears that the different doping methods do condition the structural and surface features. Furthermore, it would lead to a marked different distribution of copper species in each case.

The reduction behavior of metal species in catalyst support can be monitored by the H_2-TPR technique.[42] In Figure 8 we show the reduction profile of selected samples from different doping methods. Since TiO_2 reduction hardly happens at a lower temperature than 500 °C, the observed peaks below this temperature can be exclusively related to CuOx species. From the obtained TPR curves it is clear that a complex mixture of Cu species is present in both series. The reduction of TPR peaks below 250 °C have been interpreted by some authors to be the result of smaller CuO particles and/or highly dispersed CuO particles. Thus, the first reduction peak at around 165 °C found in both series could be attributed to the reduction of highly dispersed CuO weakly interacting with the support. In this sense, Kundakovic et al. reported that lower loading doping of copper on CeO_2 and ZrO_2 leads to a higher dispersion of Cu species which exhibit lower reduction peak.[43] For impregnated series, the peak at ca. 200 °C could be associated with the reduction of larger size CuO which weakly interacts with the support.[44−46] As it can be observed, the chemically reduced series exhibits similar TPR curves independently of the TiO_2 support (Figure 8b). It might be assumed that the distribution and nature of surface copper species are similar in both cases. As it can be noticed, a sharp H_2 consumption is observed at such low temperature as 150 °C. This would imply that in this series highly reducible copper species are present, indicating the presence of highly disperse Cu species weakly interacting with TiO_2 support. In this sense, Kurr et al. stated that the shift to higher reduction temperatures as well as a pronounced broadening of the reduction peaks would indicate larger and less dispersed copper particles.[47] This is the case of impregnated samples, Cu1STi and Cu1Ti (Figure 8a). The additional peak located at higher temperature (280 °C−350 °C) was caused by the reduction of bulk CuO.[45,46] This remarked difference in the reduction temperature between both series may be due to the particular features of copper species in the impregnated series. We have to take into account that surface copper suffers a complex evolution during calcination within the impregnated series. Indeed, such evolution clearly conditions the reducibility of copper species present in this series. Moreover, the broad TPR peak observed for Cu1STi and Cu3STr samples at around 360 °C could be related to low reducible copper species probably associated with residual surface sulfates. Samples obtained from a chemical reduction

dx.doi.org/10.1021/cs500865y | ACS Catal. 2014, 4, 3320−3329

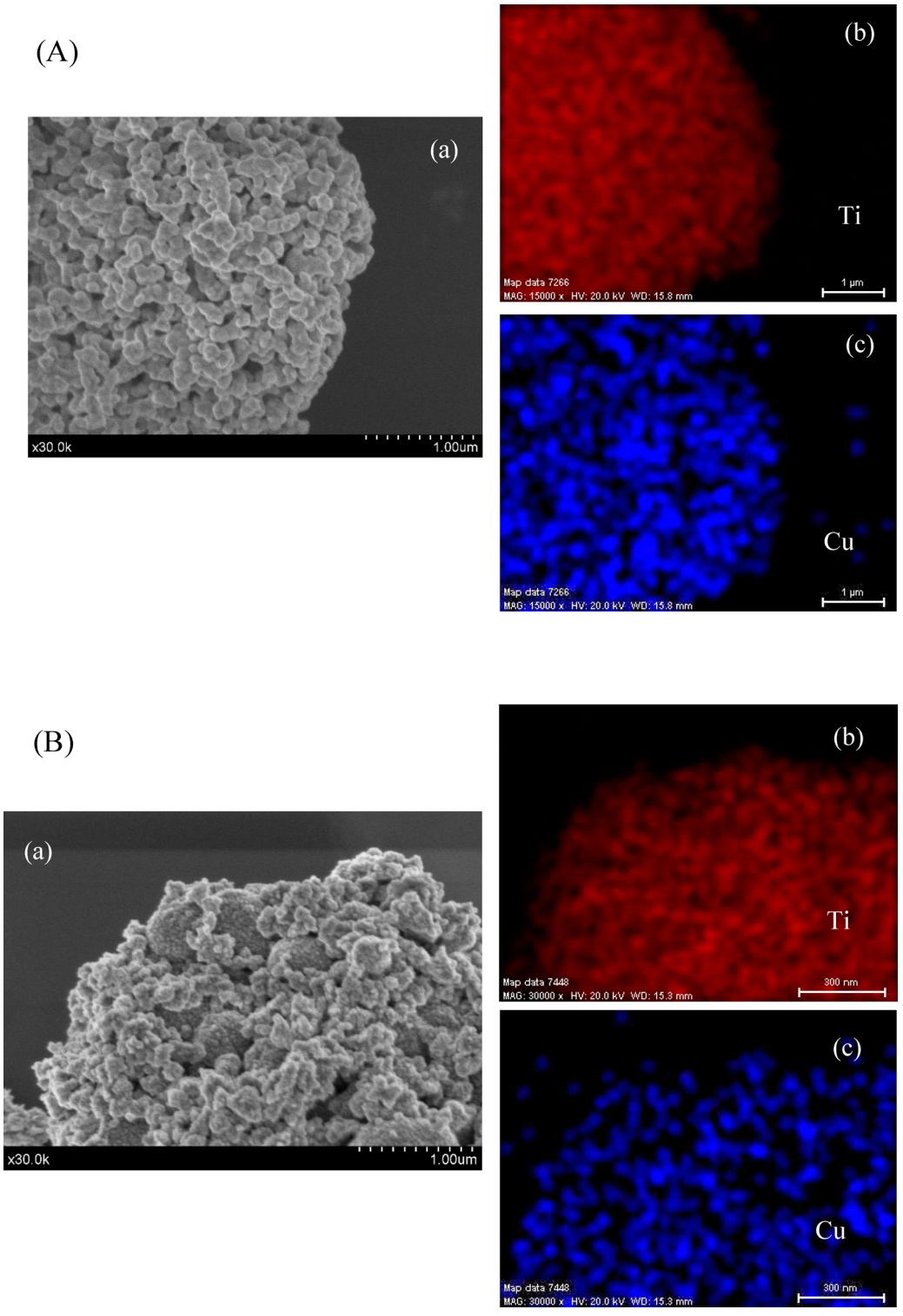

Figure 6. A) FE-SEM image of a) the Cu1STi sample and b-c) EDS mapping data for Ti and Cu. B) FE-SEM image of a) the Cu3STr sample and b-c) EDS mapping data for Ti and Cu.

method show similar TPR profiles independently of the TiO_2 support.

The determination of the nature and oxidation state of copper species has been normally accomplished using the XPS technique and in particular by means of the Cu $2p_{3/2}$ and LMM Auger peaks study.[48,49] In Figure 9 we show the Cu 2p spectra for selected samples from both series. It is worthy to note first the significant differences regarding the Cu species in both series. In all cases, the Cu 2p curve is formed by two peaks located at ca. 932 and 934 eV which can be ascribed to Cu^{1+} and Cu^{2+}, respectively.[50] In addition, the appearance of a shakeup satellite at ca. 943 eV, which is directly related to the Cu^{2+} species, suggests that a marked difference in the Cu^{2+} and Cu^{1+} composition is also present. Thus, for simultaneous impregnated-sulfated series Cu^{1+} and Cu^{2+} species cohabit at the surface. Within impregnated-sulfated series, as copper

dx.doi.org/10.1021/cs500865y | ACS Catal. 2014, 4, 3320−3329

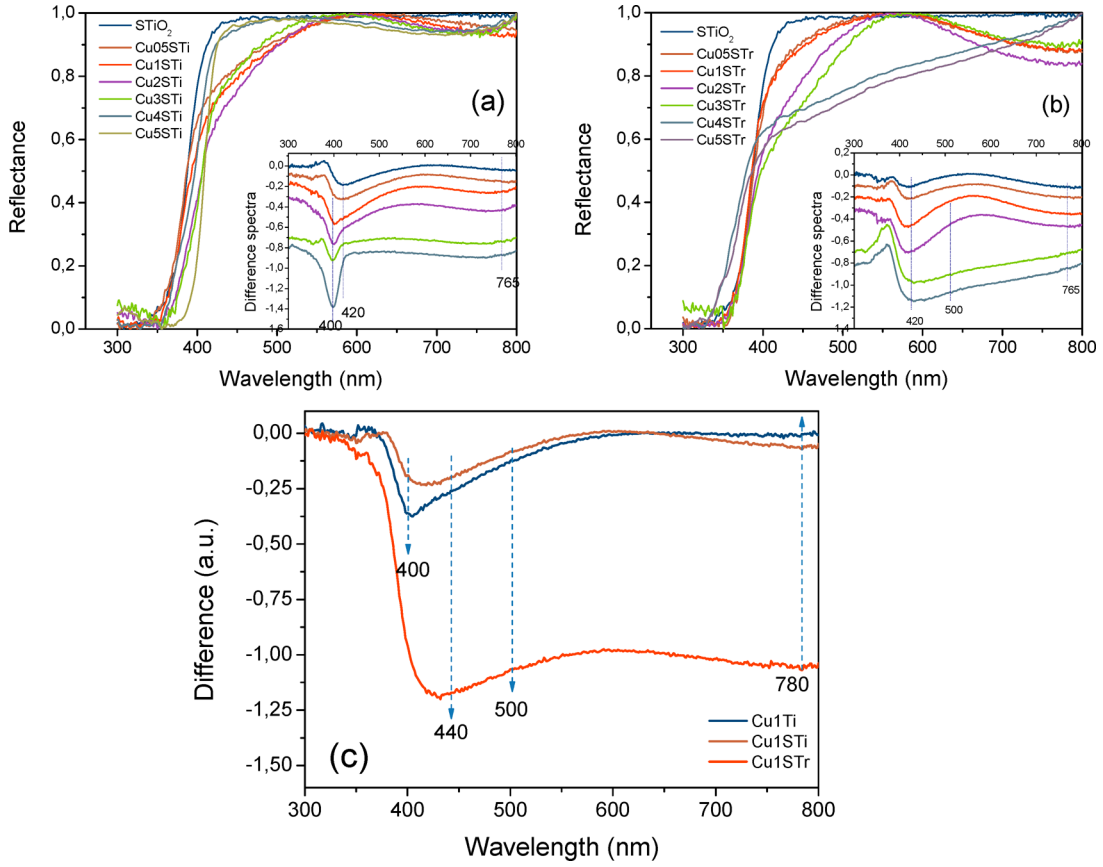

Figure 7. DRS and difference spectra of a) CuSTi and b) CuSTr series with the corresponding reference TiO_2 spectra. c) Comparison of difference spectra for 1 mol % Cu-doped catalyst from different series.

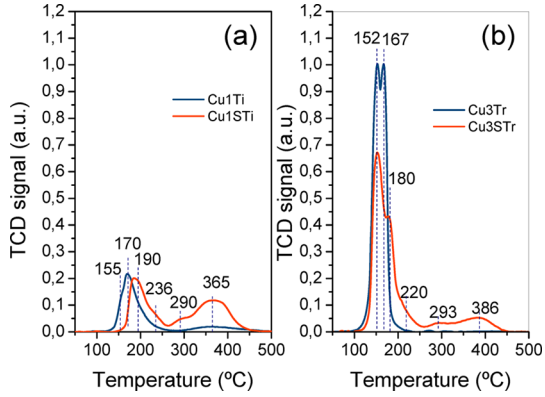

Figure 8. H_2-TPR profiles for a) CuSTi and b) CuSTr series.

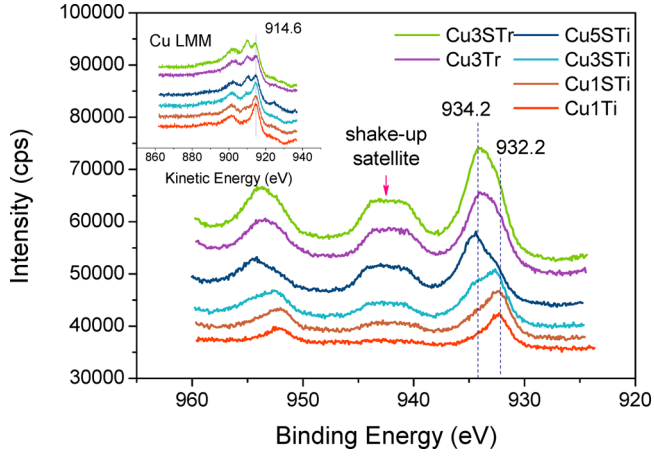

Figure 9. Cu 2p XPS spectra for Cu-doped samples from CuSTi and CuSTr series. Inset plot shows the Auger Cu LMM peak for these samples.

loading increases, the Cu^{2+} species become the main oxidation (Table 3). The effect of sulfate is clear if we compare the XPS results for Cu1STi and Cu1Ti samples. The simply impregnated sample shows the Cu^{1+} species as the predominant one. These results are undoubtedly in accordance with those from DRS and TPR above-discussed. Moreover, by observing the Cu/Ti atomic ratio it is worthy to note a strong disagreement with the nominal loading in the case of Cu1Ti. This lower surface copper content could be related with particular structural features of the Cu1Ti sample above-described. Thus, as it has been stated previously, the absence of surface sulfates during calcination would favor the rutilization process when copper is present. Moreover, the distortion of rutile lattice would evidence the incorporation of Cu^{2+} into the cell. The lower surface copper content would be explained by considering such incorporation into the structure. Since the Cu^{2+} substitution into Ti^{4+} sites would generate oxygen vacancies, surface Cu^{1+} species would be stabilized by the presence of these vacancies. In fact, the binding energy values for Ti $2p_{3/2}$ suffer a slight shift toward higher energies for sulfated TiO_2 as well as for the CuSTi series (Table 3). This shift would imply an increased positive polarity on the Ti cation, probably caused by the presence of nearby sulfate groups and even by the incorporation of Cu^{1+} ions in the TiO_2

dx.doi.org/10.1021/cs500865y | ACS Catal. 2014, 4, 3320−3329

Table 3. XPS Analysis for Different Cu-Doped TiO_2 Systems

			Cu $2p_{3/2}$ (eV)						
photocatalyst	calcination temp (°C)	Ti $2p_{3/2}$ (eV)	Cu^{1+}	Cu^{2+}	I_m/I_s	% Cu^{2+}	Cu/Ti	O/Ti	S/Ti
$STiO_2$	650	458.9						2.3	0.053
Cu1STi	650	458.6	932.3	934.0	4.2	60%	0.105	2.3	0.048
Cu3STi	650	458.6	932.3	934.1	3.4	75%	0.149	2.3	0.043
Cu5STi	650	458.5	932.5	934.6	2.2	87%	0.280	2.5	0.050
Cu3STr	650	458.2	932.2	934.0	2.4	90%	0.322	2.3	0.017
Cu1Ti	400	458.3	932.7	934.5	7.8	24%	0.065	2.1	
Cu3Tr	400	458.2	932.2	933.9	2.4	90%	0.300	2.4	

lattice. In both cases, S^{6+} and Cu^{1+} show higher electronegativity and would polarize Ti−O bonding.

This complex behavior is also observed for impregnated-sulfated samples with higher copper content. As copper doping increases, it has been observed a progressive destabilization of the anatase structure and a subsequent appearance of the rutile phase. Within this evolution, copper is similarly substitutionally incorporated into the TiO_2 structure (Table 3). However, since the amount of copper at the surface is higher, the formation of copper aggregates would increase the the Cu^{2+} fraction.

It is worthy to note that for the chemically reduced series no difference is observed between Cu3STr and Cu3Tr samples. It is clear that in this case the support does not condition the surface situation of copper. Moreover, the chemical analysis of these samples denotes similar surface copper content and close to the nominal loadings (Table 3). For these samples, Cu^{2+} arises as the predominant copper species at the surface. Thus, after chemical reduction, it can be evidenced that the final powder suffers a reoxidation process probably during the drying step. The homogeneous composition of copper species denoted from XPS analysis is also in good agreement with TPR curves. Moreover, Ti $2p_{3/2}$ binding energies appear to be similar to bare TiO_2 (458.3 eV) denoting that no interaction is present with Cu^{1+} being present in this case (Table 3).

The different photocatalytic performances observed for the studied systems can be explained by considering the structural, surface, and chemical states of copper (Scheme 1). Thus, the impregnated-sulfated series exhibits a complex situation with copper content. The sulfate presence would stabilize the TiO_2 structure as well as would retain copper at the surface. As copper loading increases the structural destabilization and rutile appearance would favor the copper insertion into the TiO_2 lattice. The simply impregnated sample (Cu1Ti) would exhibit a complex structural configuration in which copper is divided into the surface and the structure. In addition, the structural and surface features of TiO_2 support will also affect the final photocatalytic activity. Finally, copper doping by a chemical reduction method leads to a highly disperse Cu^{2+} on the surface. So, it can be said that the different performances observed for these chemically reduced samples would be explained by considering the different structural and surface features of the support. By comparing Cu1STi and Cu3STr it can be assumed that in both cases the active copper species is Cu^{2+}. The particular structural and surface properties of the support seem to strongly condition the final performance of both systems.

Scheme 1. Schematic Insight of Copper Situation on Different Samples

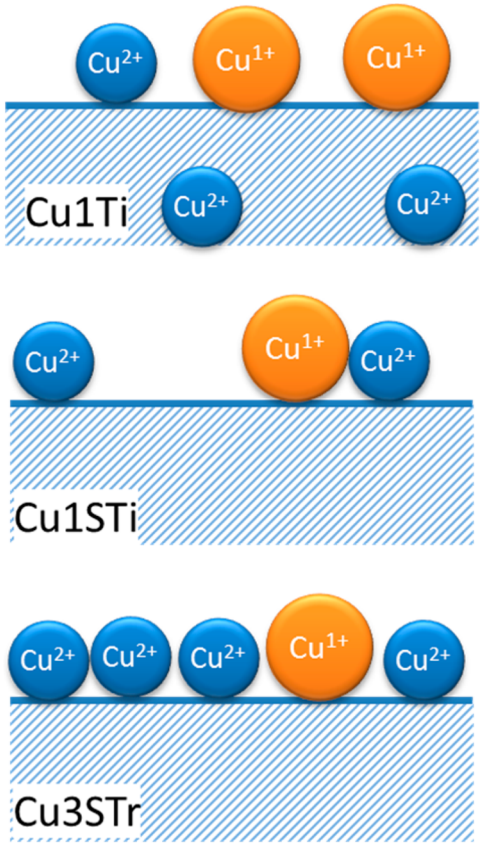

CONCLUSIONS

We have prepared a set of Cu-doped TiO_2 by a different doping method. From the wide structural and surface characterization of the studied samples we can conclude that the occurrence of highly disperse Cu^{2+} species is directly related to the higher performance of the system for the H_2 production reaction. Thus, highly disperse Cu^{2+} species would be easily reduced during the reaction forming Cu^0 sites that will act as an effective cocatalyst for a water reduction reaction. In the case of impregnated series, in addition to such Cu^0 species the presence of Cu^{2+} in the TiO_2 lattice would also participate in the electronic mechanism by enhancing to a certain extent the photogenerated charge pairs. Moreover, the presulfation treatment of the TiO_2 support clearly induces a higher photocatalytic activity. Indeed, a high temperature anatase structure, with relatively high surface area, would induce an improved charge separation and diffusion processes. The obtained photonic efficiencies for the best series are significantly higher than those reported for similar systems. By a simple doping method we have obtained a notable photocatalytic activity. So, it is clear that the understanding of a

dx.doi.org/10.1021/cs500865y | ACS Catal. 2014, 4, 3320−3329

chemical and structural situation of active species is crucial to design highly active systems.

■ ASSOCIATED CONTENT

Supporting Information

EDX analysis of selected samples. This material is available free of charge via the Internet at http://pubs.acs.org.

■ AUTHOR INFORMATION

Corresponding Author

*E-mail: gcolon@icmse.csic.es.

Notes

The authors declare no competing financial interest.

■ ACKNOWLEDGMENTS

We acknowledge the financial support by Junta de Andalucía and CICYT through FQM-4570 and ENE2011-24412 projects. S. Obregón thanks CSIC for the concession of a JAE-Pre grant.

■ REFERENCES

(1) Kubacka, A.; Fernández-García, M. *Chem. Rev.* **2012**, *112*, 1555−1614.
(2) Cates, E. L.; Chinnapongse, S. L.; Kim, J. H. *Environ. Sci. Technol.* **2012**, *46*, 12316−12328.
(3) Hwang, J. S.; Chang, J. S.; Park, S. E.; Ikeue, K.; Anpo, M. *Top. Catal.* **2005**, *35*, 311−319.
(4) Vinu, R.; Madras, G. *Curr. Org. Chem.* **2013**, *17*, 2538−2558.
(5) Colmenares, J. C.; Luque, R. *Chem. Soc. Rev.* **2014**, *43*, 765−778.
(6) Grätzel, M.; Howe, R. F. *J. Phys. Chem.* **1990**, *94*, 2566−2572.
(7) Li, X.; Yue, P. L.; Kutal, C. *New J. Chem.* **2003**, *8*, 1264−1269.
(8) Naldoni, A.; D'Arienzo, M.; Altomare, M.; Marelli, M.; Scotti, R.; Morazzoni, F.; Selli, E.; Dal Santo, V. *Appl. Catal,. B* **2013**, *130−131*, 239−248.
(9) Puga, A. V.; Forneli, A.; García, H.; Corma, A. *Adv. Funct. Mater.* **2014**, *24*, 241−248.
(10) Su, R.; Tiruvalam, R.; Logsdail, A. J.; He, Q.; Downing, C. A.; Jensen, M. T.; Dimitratos, N.; Kesavan, L.; Wells, P. P.; Bechstein, R.; Jensen, H. H.; Wendt, S.; Catlow, C. R. A.; Kiely, C. J.; Hutchings, G. J.; Besenbacher, F. *ACS Nano* **2014**, *8*, 3490−3497.
(11) Pulido Melián, E.; Nereida Suárez, M.; Jardiel, T.; Doña Rodríguez, J. M.; Caballero, A. C.; Araña, J.; Calatayud, D. G.; González Díaz, O. *Appl. Catal., B* **2014**, *152−153*, 192−201.
(12) Dholam, R.; Patel, N.; Adami, M.; Miotello, A. *Int. J. Hydrogen Energy* **2009**, *34*, 5337−5346.
(13) Ampelli, C.; Passalacqua, R.; Genovese, C.; Perathoner, S.; Centi, G.; Montini, T.; Gombac, V.; Delgado Jaen, J. J.; Fornasiero, P. *RSC Adv.* **2013**, *3*, 21776−21788.
(14) Oros-Ruiz, S.; Zanella, R.; Collins, S. E.; Hernández-Gordillo, A.; Gómez, R. *Catal. Commun.* **2014**, *47*, 1−6.
(15) Wang, Z.; Liu, Y.; Martin, D. J.; Wang, W.; Tang, J.; Huang, H. *Phys. Chem. Chem. Phys.* **2013**, *15*, 14956−14960.
(16) Hu, S.; Zhou, F.; Wang, L.; Zhang, J. *Catal. Commun.* **2011**, *12*, 794−797.
(17) Xi, Z.; Li, C.; Zhang, L.; Xing, M.; Zhang, J. *Int. J. Hydrogen Energy* **2014**, *39*, 6345−6353.
(18) Xu, S.; Sun, D. D. *Int. J. Hydrogen Energy* **2009**, *34*, 6096−6104.
(19) Gombac, V.; Sordelli, L.; Montini, T.; Delgado, J. J.; Adamski, A.; Adami, G.; Cargnello, M.; Bernal, S.; Fornasiero, P. *J. Phys. Chem. A* **2010**, *114*, 3916−3925.
(20) Korzhak, A. V.; Ermokhina, N. I.; Stroyuk, A. L.; Bukhtiyarov, V. K.; Raevskaya, A. E.; Litvin, V. I.; Kuchmiy, S. Y.; Ilyin, V. G.; Manorik, P. A. *J. Photochem. Photobiol., A* **2008**, *198*, 126−134.
(21) Colón, G.; Sánchez-España, J. M.; Hidalgo, M. C.; Navío, J. A. *J. Photochem. Photobiol., A* **2006**, *179*, 20−27.
(22) Monti, D. A.; Baiker, A. *J. Catal.* **1983**, *83*, 323.
(23) Malet, P.; Caballero, A. *J. Chem. Soc., Faraday Trans. I* **1988**, *84*, 2369−2375.
(24) Montini, T.; Gombac, V.; Sordelli, L.; Delgado, J. J.; Chen, X.; Adami, G.; Fornasiero, P. *ChemCatChem.* **2011**, *3*, 574−577.
(25) Khemthong, P.; Photai, P.; Grisdanurak, N. *Int. J. Hydrogen Energy* **2013**, *38*, 15992−15999.
(26) Reddy, J. K.; Lalitha, K.; Reddy, P. V. L.; Sadanandam, G.; Subrahmanyam, M.; Kumar, V. D. *Catal. Lett.* **2014**, *144*, 340−346.
(27) Colón, G.; Hidalgo, M. C.; Munuera, G.; Ferino, I.; Cutrufello, M. G.; Navío, J. A. *Appl. Catal., B* **2006**, *63*, 45−59.
(28) Hidalgo, M. C.; Maicu, M.; Navío, J. A.; Colón, G. *Appl. Catal., B* **2008**, *81*, 49−55.
(29) Hidalgo, M. C.; Maicu, M.; Navío, J. A.; Colón, G. *J. Phys. Chem. C* **2009**, *113*, 12840−12847.
(30) Gombac, V.; Sordelli, L.; Montini, T.; Delgado, J. J.; Adamski, A.; Adami, G.; Cargnello, M.; Bernal, S.; Fornasiero, P. *J. Phys. Chem. A* **2010**, *114*, 3916−3925.
(31) Xu, S.; Du, A. J.; Liu, J.; Ng, J.; Sun, D. D. *Int. J. Hydrogen Energy* **2011**, *36*, 6560−6568.
(32) Colón, G.; Hidalgo, M. C.; Navío, J. A.; Kubacka, A.; Fernández-García, M. *Appl. Catal., B* **2009**, *90*, 633−641.
(33) Obregón, S.; Kubacka, A.; Fernández-García, M.; Colón, G. *J. Catal.* **2013**, *299*, 298−306.
(34) Choudhury, B.; Dey, M.; Choudhury, A. *Int. Nano Lett,* **2013**, *3*, 55.
(35) Navas, J.; Sánchez-Coronilla, A.; Aguilar, T.; Hernández, N. C.; de los Santos, D. M.; Sánchez-Márquez, J.; Zorrilla, D.; Fernández-Lorenzo, C.; Alcántara, R.; Martín-Calleja, J. *Phys. Chem. Chem. Phys.* **2014**, *16*, 3835−3845.
(36) Parker, J. C.; Siegel, R. W. *Appl. Phys. Lett.* **1990**, *57*, 943−945.
(37) Montanari, B.; Vaccari, A.; Gazzano, M.; Kdher, P.; Papp, H.; Pasel, J.; Dziembaj, R.; Makowski, W.; Lojewski, T. *Appl. Catal., B* **1997**, *13*, 205−217.
(38) Lin, W.; Frei, H. *J. Am. Chem. Soc.* **2005**, *127*, 1610−1611.
(39) Lenglet, M.; Kartouni, K.; Delahaye, D. *J. Appl. Electrochem.* **1991**, *21*, 697−702.
(40) Crivello, M.; Pérez, C.; Herrero, E.; Ghione, G.; Casuscelli, S.; Rodríguez-Castellón, E. *Catal. Today* **2005**, *107−108*, 215−222.
(41) Velu, S.; Suzuki, K.; Okazaki, M.; Kapoor, M. P.; Osaki, T.; Ohashi, F. J. *J. Catal.* **2000**, *194*, 373−384.
(42) Chen, C. S.; You, J. H.; Lin, J. C.; Chen, Y. Y. *Catal. Commun.* **2008**, *9*, 2381−2385.
(43) Kundakovic, Lj.; Flytzani-Stepahanopoulos, M. *Appl. Catal., A* **1998**, *171*, 13−29.
(44) Wang, S. P.; Zhang, T. Y.; Su, Y.; Wang, S. R.; Zhang, S. M.; Zhu, B. L.; Wu, S. H. *Catal. Lett.* **2008**, *121*, 70−76.
(45) Boccuzzi, F.; Martra, G.; Partipilo Papalia, C.; Ravasio, N. *J. Catal.* **1999**, *184*, 327−334.
(46) Perkas, N.; Gunawan, P.; Amirian, G.; Wang, Z.; Zhong, Z.; Gedanken, A. *Phys. Chem. Chem. Phys.* **2014**, *16*, 7521−7530.
(47) Kurr, P.; Kasatkin, I.; Girgsdies, F.; Trunschke, A.; Schlögl, R.; Ressler, T. *Appl. Catal., A* **2008**, *348*, 153−164.
(48) Espinós, J. P.; Morales, J.; Barranco, A.; Caballero, A.; Holgado, J. P.; González-Elipe, A. R. *J. Phys. Chem. B* **2002**, *106*, 6921−6929.
(49) Tian, H.; Zhang, X. L.; Scott, J.; Nga, C.; Amal, R. *J. Mater. Chem. A* **2014**, *2*, 6432−6438.
(50) Zhu, M.; Du, M. L.; Yu, D. L.; Wang, Y.; Wang, N. L.; Zou, M. L.; Zhang, M.; Fu, Y. Q. *J. Mater. Chem. A* **2013**, *1*, 919−923.